

Restoring Coherence Lost to a Slow Interacting Mesoscopic Bath

Wang Yao,^{*} Ren-Bao Liu,[†] and L. J. Sham

Department of Physics, University of California San Diego, La Jolla, California 92093-0319

(Dated: October 15, 2018)

For a two-state quantum object interacting with a slow mesoscopic interacting spin bath, we show that a many-body solution of the bath dynamics conditioned on the quantum-object state leads to an efficient control scheme to recover the lost quantum-object coherence through disentanglement. We demonstrate the theory with the realistic problem of one electron spin in a bath of many interacting nuclear spins in a semiconductor quantum dot. The spin language is easily generalized to a quantum object in contact with a bath of interacting multi-level quantum units with the caveat that it is mesoscopic and its dynamics is slow compared with the quantum object.

Coherent superposition of states of a quantum object is the wellspring of quantum properties and key to quantum technology. Decoherence of a quantum object results from the entanglement with an environment by coupled dynamics [1, 2, 3]. Amelioration of decoherence becomes important in any sustained quantum process. Different types of amelioration include dynamical decoupling [4, 5, 6], decoherence-free subspace [7], quantum error correction (for a review, see [8]), and feedback control [9].

We offer an alternate approach to the restoration of coherence based on the theory that control of the quantum object can direct the quantum evolution of the bath to disentangle the object from the bath. The operation resembles the spin echo schemes [10] but it removes the pure decoherence due to bath interaction dynamics as well as the inhomogeneous broadening effect. The key is that the environment is effectively a mesoscopic system, i.e., the number of particles N is small enough for the timescale of the quantum object decoherence to be much smaller than its energy relaxation time T_1 while large enough for ergodicity, specifically for the Poincaré period to be effectively infinite as compared to T_1 .

^{*}Presently at Department of Physics, The University of Texas, Austin, Texas 78712-0264

[†]Presently at Department of Physics, The Chinese University of Hong Kong, Hong Kong, China

The theoretical demonstration of coherence restoration uses one electron spin in a semiconductor quantum dot of many ($N \sim 10^6$) nuclear spins, which serves as a paradigmatic system of a two-level system in a bath of interacting spins for decoherence physics [11] and for spin-based quantum technology [12, 13]. Electron spin decoherence due to the hyperfine interaction with the nuclear spins has been much studied (see [14] and references therein). Theories of the effect of interaction between nuclear spins on the electron decoherence have recently appeared [3, 15]. Our theory of coherence recovery by disentanglement is based on the previous finding [3] that the mesoscopic bath of slow dynamics is well described by a simple pseudospin model for the particle pair interaction in the bath.

We start by defining the decoherence process in a simple quantum prescription. The model for the coupled spin-bath system is a localized electron of spin $1/2$ coupled to a bath of finite N mutually interacting nuclei with spin j in a magnetic field. The isolation of the electron spin plus the meso-bath, in the timescale of the total processing duration T_p , from the rest of universe arises out of their weak coupling with the outside. The initial state of the electron spin, $|\varphi^s(0)\rangle = C_+|+\rangle + C_-|-\rangle$, is prepared as a coherent superposition of the spin up and down states $|\pm\rangle$ in an external magnetic field. The state of the total system of the spin plus bath at that instant forms an *unentangled* state, $|\Psi(0)\rangle = |\varphi^s(0)\rangle \otimes |\mathcal{J}\rangle$. It evolves over time t to the *entangled* $|\Psi(t)\rangle = C_+(t)|+\rangle \otimes |\mathcal{J}^+(t)\rangle + C_-(t)|-\rangle \otimes |\mathcal{J}^-(t)\rangle$ where the bath states $|\mathcal{J}^\pm(t)\rangle$ are different. The electron spin state is now given by the reduced density matrix by tracing over the bath states, $\rho_{\sigma,\sigma'}^s(t) = C_{\sigma'}^*(t)C_{\sigma}(t)\langle\mathcal{J}^{\sigma'}(t)|\mathcal{J}^{\sigma}(t)\rangle$, $\sigma, \sigma' = \pm$. The environment-driven shifting between $\rho_{+,+}^s$ and $\rho_{-,-}^s$ is longitudinal relaxation. Either off-diagonal element gives a measure of the coherence of the spin. The longitudinal relaxation contributes to the decoherence. When this contribution is removed, the remaining decoherence is called pure dephasing. For applications in quantum technology, the longitudinal relaxation time T_1 can be made much longer than the processing duration T_p by a choice of system and of the electron Zeeman splitting much larger than the dominant excitation energies in the bath and the spin-bath coupling strength [17, 18, 19]. When the cause of spin flip is removed, the reduced Hamiltonian of the whole system is in the form diagonal in the electron spin basis, $\hat{H} = |+\rangle\langle+| \otimes \hat{H}^+ + |-\rangle\langle-| \otimes \hat{H}^-$. The bath evolves under the Hamiltonians \hat{H}^\pm into separate states $|\mathcal{J}^\pm(t)\rangle \equiv e^{-i\hat{H}^\pm t}|\mathcal{J}\rangle$ depending on the electron basis states $|\pm\rangle$. Pure dephasing is then measured by $\mathcal{L}_{+,-}^s(t) = |\langle\mathcal{J}|e^{i\hat{H}^-t}e^{-i\hat{H}^+t}|\mathcal{J}\rangle|$. The electron spin coherence may be restored by exploiting the dependence of the bath dynamics on

the electron spin states to make the bifurcated bath pathways intersect at a later time, i.e., $|\mathcal{J}^+(t)\rangle = |\mathcal{J}^-(t)\rangle$, leading to disentanglement.

At temperature ($\sim 10\text{mK}-1\text{K}$) \gg the nuclear Zeeman energy ω_n ($\sim \text{mK}$) \gg nuclear spin interaction ($\sim \text{nK}$), the nuclear bath initially has no off-diagonal coherence and is described by $\sum_{\mathcal{J}} P_{\mathcal{J}} |\mathcal{J}\rangle \langle \mathcal{J}|$ where $|\mathcal{J}\rangle \equiv \bigotimes_n |j_n\rangle$, j_n is the quantum number for \hat{J}_n^z , the component of the n th nuclear spin along z (the magnetic field direction), and $P_{\mathcal{J}}$ gives thermal distribution. The essence of electron decoherence is contained in the consideration of each pure bath state $|\mathcal{J}\rangle$ and later the ensemble average over \mathcal{J} is included. The transverse interaction $\hat{J}_n^+ \hat{J}_m^-$ between two bath spins creates the pair-flip excitation, $|j_n\rangle |j_m\rangle \rightarrow |j_n+1\rangle |j_m-1\rangle$. We sort out all such elementary excitations from the “vacuum” state $|\mathcal{J}\rangle$ and denote each by the flip-process of a *pseudospin* 1/2 indexed by k : $|\uparrow_k\rangle \rightarrow |\downarrow_k\rangle$, characterized by the energy cost $\pm E_k + D_k$ and the transition matrix element $\pm A_k + B_k$ depending on the electron $|\pm\rangle$ state. $\pm E_k$ ($\sim \mathcal{A}/N$) is from the longitudinal interaction of the form $\hat{S}^z \hat{J}_n^z$ between the electron spin \hat{S}^z and each of the two nuclear spins [20]. A_k ($\sim \mathcal{A}^2/N^2\Omega$, Ω being the electron Zeeman energy) is the extrinsic coupling between two nuclear spins mediated by virtual spin-flips of the single electron [3]. Its dependence on the number of particles in the bath signifies its mesoscopic nature. B_k is due to the transverse part of the intrinsic (e.g. dipolar) interaction between the nuclear spins with strength $\sim b$. The extrinsic interaction A_k couples any two spins in the meso-bath, as opposed to the finite-range intrinsic interaction B_k . D_k ($\sim b$) is due to the longitudinal part of the intrinsic nuclear interaction.

In the nuclear bath with the descending order of parameters, $\Omega \gg \omega_n \gg \mathcal{A}/N \gg b$, the bath dynamics is slow and the density of pair-flip excitations created from the “vacuum” state $|\mathcal{J}\rangle$ is much less than unity in timescale of interest [3]. The excitations are almost always spatially separated, leading to the pair-correlation approximation [3, 15] which treats pair-flips as independent of each other. The bath is then driven by the effective Hamiltonian derived from the first-principles interactions [3],

$$\hat{H}^{\pm} = \sum_k \hat{\mathcal{H}}_k^{\pm} \equiv \sum_k \mathbf{h}_k^{\pm} \cdot \hat{\boldsymbol{\sigma}}_k / 2, \quad (1)$$

where $\hat{\boldsymbol{\sigma}}_k$ is the Pauli matrix for pseudospin k driven by a pseudo-magnetic field $\mathbf{h}_k^{\pm} \equiv (2B_k \pm 2A_k, 0, D_k \pm E_k)$ depending on the electron $|\pm\rangle$ state.

From the justification that correlations of more than two spins are negligible [3], we derive

the restrictions which the decoherence timescale places on the size of the bath N , given by $N^2 b^2 \mathcal{A}^{-2} \ll 1 \ll \min(\sqrt{N}, N^4 b^2 \Omega^4 \mathcal{A}^{-6})$, to be established below. The upper bound for N distinguishes the bath from a macroscopic system. It comes from the dominance of the pair correlation in the interaction dynamics of the bath spins over the correlations of more than two particles due to the intrinsic interaction. The lower bound, $N^4 b^2 \Omega^4 \mathcal{A}^{-6} \gg 1$, is by a similar consideration but due to the extrinsic interaction of the bath spins. The lower bound $\sqrt{N} \gg 1$ simply signifies the necessary statistics for decoherence. In the case of the electron spin in a GaAs quantum dot, the theory is well justified for $10^8 \geq N \geq 10^4$ which covers quantum dots of all practical sizes.

The theory of the interacting nuclear spin dynamics dominated by the pair excitation in the form of the pseudospin evolution leads to a simple physical picture of coherence decay and restoration. The initial unpolarized bath state $|\mathcal{J}\rangle = \bigotimes_n |j_n\rangle$ can be replaced by the pseudospin product state $\bigotimes_k |\uparrow_k\rangle$. Each pseudospin, representing a nuclear spin states pair, initially points along the pseudospin $+z$ -axis and then precesses about the pseudo-magnetic field \mathbf{h}_k^\pm , $|\psi_k^\pm\rangle \equiv e^{-\frac{i}{2}\mathbf{h}_k^\pm \cdot \hat{\boldsymbol{\sigma}}_k t} |\uparrow_k\rangle$, depending on the electron $|\pm\rangle$ state. Thus, the electron spin coherence is measured by the divergence of the pseudospin paths, $\mathcal{L}_{+,-}^s(t) = \prod_k |\langle\psi_k^-|\psi_k^+\rangle| \cong e^{-\sum_k \delta_k^2/2}$. $\delta_k \equiv \sqrt{1 - |\langle\psi_k^-|\psi_k^+\rangle|^2}$ is the geometric distance between the two conjugate pseudospin paths on Bloch sphere.

Now we examine the consequences of the pseudospin echo. A fast π -pulse applied at $t = \tau$ to flip the electron spin [21] would cause the pseudo-spin evolution

$$|\psi_k^\pm(t)\rangle = e^{-\frac{i}{2}\mathbf{h}_k^\mp \cdot \hat{\boldsymbol{\sigma}}_k (t-\tau)} e^{-\frac{i}{2}\mathbf{h}_k^\pm \cdot \hat{\boldsymbol{\sigma}}_k \tau} |\uparrow\rangle. \quad (2)$$

To find out how to control the decoherence, we neglect for the time being the diagonal nuclear spin interaction D_k , which contributes to the same component of the pseudo-magnetic field as E_k but much smaller. Because the pseudo-fields dominated by the extrinsic nuclear spin interaction, $\mathbf{h}_k^\pm \equiv \pm(2A_k, 0, E_k)$, invert exactly into each other, disentanglement of the electron spin from the affected bath spin pairs follows at 2τ as in the classic spin echo to remove the inhomogeneous broadening effect. The pseudo-fields dominated by the intrinsic interaction, $\mathbf{h}_k^\pm \equiv (2B_k, 0, \pm E_k)$, do not exactly invert under the influence of the electron spin flip and the resultant pseudospin trajectories are illustrated in Fig. 1(a). Disentanglement from the affected nuclear pairs and, hence, recovery of the electron spin coherence occurs,

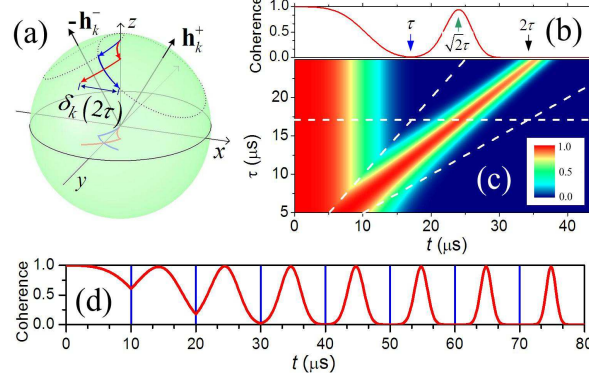


FIG. 1: (a) Precession of the conjugated pseudo-spin vectors under single-pulse control. Red (blue) trajectory denotes when the electron state is $|+\rangle$ ($|-\rangle$). (b) Electron spin coherence $\mathcal{L}_{+,-}^s(t)$ under the control of a single flip pulse applied at $\tau = 17 \mu\text{s}$ (indicated with the blue arrow). The revived coherence peaks at $\sqrt{2}\tau$ (indicated by the green arrow) while coherence at the conventional spin echo time 2τ (indicated with the black arrow) is negligible. (c) Contour plot of the electron spin coherence $\mathcal{L}_{+,-}^s$ under single pulse control as a function of time t and the pulse delay time τ (indicated by the left tilted line). The restoration of the coherence is pronounced at $\sqrt{2}\tau$ whereas no coherence peak is visible at the conventional echo time 2τ (indicated by the right tilted line). The horizontal line is the cut for the curve in (c). (d) Electron spin coherence with a sequence of π -rotations (indicated by blue vertical lines) at intervals of $\tau = 10 \mu\text{s}$. The numerical evaluation is performed on a GaAs dot with thickness $d = 8.5 \text{ nm}$ in growth direction $[001]$ and lateral Fock-Darwin radius $r_0 = 25 \text{ nm}$, on the large- N side of the mesoscopic regime where the intrinsic nuclear interaction dominates [3]. $\mathbf{B}_{\text{ext}} = 10 \text{ T}$ along the $[110]$ direction. The electron g -factor is -0.44 . The random choice of the initial bath state $|\mathcal{J}\rangle \equiv \bigotimes_n |j_n\rangle$ from a thermal ensemble at temperature $T = 1 \text{ K}$ makes negligible difference to the results.

by the rotation kinematics, at time $\sqrt{2}\tau$, distinct from the classic echo. Fig. 1(b,c) give the computed results for the electron spin coherence in a dot of 10^6 nuclear spins in GaAs which reveals the coherence recovery after a flip of the electron spin at a range of values for τ , even after the coherence has apparently vanished.

Furthermore, the coherence may be restored by a sequence of electron spin flips. For example, with a sequence of π -pulses evenly spaced with interval τ , the disentanglement from the bath will occur at $\sqrt{n(n+1)}\tau$ between the n th and the $(n+1)$ th pulses, as illustrated in Fig. 1(d). Consider the correction from the small term D_k in the pseudo-fields, the residue decoherence, at the disentanglement point $\sqrt{n(n+1)}\tau$, is measured by $\delta_k^2 \sim (E_k B_k D_k \tau^3)^2$. Compared to the free-induction decay [3] where $\delta_k^2(\tau) \sim E_k^2 B_k^2 \tau^4$, the decoherence is reduced by a factor of $\sim D_k^2 \tau^2$ ($\sim 10^{-4}$ for $\tau \sim 10 \mu\text{s}$).

Ensemble average over the mixed bath states is necessary in two scenarios, namely, observation of decoherence of an ensemble of quantum objects and observation of a single

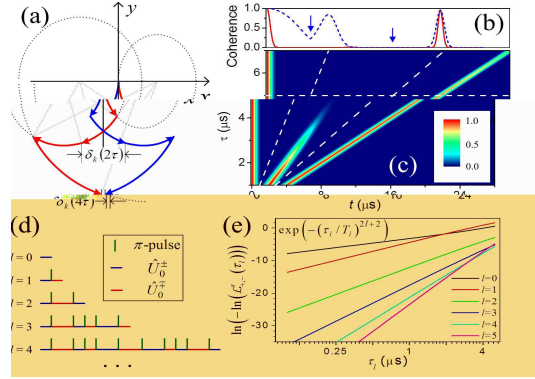


FIG. 2: (a) Pseudo-spin trajectories (projected on x - y plane) driven by intrinsic nuclear interaction with two π -rotations of the electron spin at τ and 3τ . (b) Evolution of the electron spin coherence under two-pulse control with $\tau = 5 \mu\text{s}$. The dashed blue line denotes the pure state dynamics part $\mathcal{L}_{+,-}^s$ and the solid red line includes the inhomogeneous broadening factor $\mathcal{L}_{+,-}^0$. The blue arrows indicate the times of the electron spin flip. (c) Contour plot of the ensemble-averaged electron spin coherence under the two-pulse control. The tilted lines indicate the pulse times and the horizontal line is the cut for the curve in (b). In (b) and (c), we have artificially set the ensemble dephasing time T_2^* in $\mathcal{L}_{+,-}^0$ to $0.5 \mu\text{s}$, about 100 times greater than its realistic value, to make the echo visible in the plot. (d) Concatenated pulse sequences. The $(l+1)$ th order sequence is constructed by two subsequent l th order sequences, with a pulse inserted if l is even. (e) Dependence of echo magnitude on the echo delay time τ_l under the control of the concatenated pulse sequences in ensemble measurement. The quantum dot is the same as in Fig. 1 except smaller, $d = 2.8 \text{ nm}$ and $r_0 = 15 \text{ nm}$. The nuclear bath is assumed initially in thermal equilibrium at $T = 1 \text{ K}$.

quantum object repeated in a time sequence [21, 22, 23, 24]. The coherence of the electron spin is now $\rho_{+,-}(t) = C_-^* C_+ \mathcal{L}_{+,-}^s(t) \times \mathcal{L}_{+,-}^0(t)$, where $\mathcal{L}_{+,-}^0(t) \equiv \sum_{\mathcal{J}} P_{\mathcal{J}} e^{-i\phi_{\mathcal{J}}(t)}$ is the inhomogeneous broadening factor due to the probability distribution $P_{\mathcal{J}}$ of the initial bath state $|\mathcal{J}\rangle$ (different nuclear bath state may result in different Overhauser energy-splitting $\mathcal{E}_{\mathcal{J}}$ of the electron) [3]. $\phi_{\mathcal{J}}(t) = \mathcal{E}_{\mathcal{J}} [\tau_1 - (\tau_2 - \tau_1) + \dots + (-1)^n(t - \tau_n)]$ under the control of a sequence of π -rotations on electron spin at τ_1, τ_2, \dots , and τ_n . The coherence factor $\mathcal{L}_{+,-}^s(t)$ is insensitive, up to a factor of $1/\sqrt{N} \ll 1$, to the selection of initial bath state $|\mathcal{J}\rangle \equiv \bigotimes_n |j_n\rangle$ (verified by numerical evaluations), and is taken out of the summation [3].

Both the inhomogeneous broadening and the pure decoherence due to the extrinsic bath spin interaction are shown to be removed at the classic spin echo time 2τ in contrast to the unusual recovery time of $\sqrt{2}\tau$ in the case of intrinsic bath spin interaction. We need a pulse sequence to produce a time where the decoherence from all three sources can be removed. A solution is a two-pulse control. Fig. 2(a) shows that, after a second electron

spin flip at 3τ , the paths of the two pseudospin states corresponding to the electron $|\pm\rangle$ states driven by the intrinsic nuclear spin pair interaction cross again at 4τ , coinciding with the secondary spin echo time for the other two causes. This two pulse sequence is well-known as Carr-Purcell sequence in NMR spectroscopies [10]. The residual decoherence at $t = 4\tau$ is $\delta_k^2 \sim 16 (E_k B_k - A_k D_k)^2 D_k^2 \tau^6$. The restoration by two-pulse control of coherence in the presence of both pure and ensemble decoherence is demonstrated by the results of numerical evaluation shown in Fig. 2(b,c). The electron spin coherence is restored at 4τ by the second pulse even when the first spin-echo at 2τ has completely vanished, illustrating the remarkable observation [25] that the absence of spin echo does not mean irreversible loss of coherence.

The power of concatenation of pulse sequences has been shown in the context of dynamical decoupling in quantum computation [4]. Similarly, the control of disentanglement of the bath states from the quantum object may be enhanced by concatenation. The pseudo-spin evolution with the two-pulse control of the quantum object can be constructed recursively from the free-induction evolution $\hat{U}_0^\pm = e^{-i\mathbf{h}_k^\pm \cdot \hat{\boldsymbol{\sigma}}_k \tau/2}$, by the concatenation, $\hat{U}_l^\pm = \hat{U}_{l-1}^\mp \hat{U}_{l-1}^\pm$, $l = 1, 2$. The process can be extended by iteration, Fig. 2(d), to any level, $\hat{U}_l^\pm = e^{-i\boldsymbol{\theta}_l^\pm \cdot \hat{\boldsymbol{\sigma}}_k/2}$, where $\boldsymbol{\theta}_l^\pm$ is the rotation vector along the axis of rotation through an angle θ_l^\pm . Disentanglement occurs at $\tau_l \equiv 2^l \tau$ coinciding with the classic spin echo. For small θ_l^\pm , the recursion relation is $\boldsymbol{\theta}_{l+1}^\pm = \boldsymbol{\theta}_l^+ + \boldsymbol{\theta}_l^- \mp \boldsymbol{\theta}_l^+ \times \boldsymbol{\theta}_l^-$. At each iteration, the rotation vectors of the conjugate pseudo-spin states have their mean $(\boldsymbol{\theta}_l^+ + \boldsymbol{\theta}_l^-)/2$ increased by a factor of 2 and their difference $(\boldsymbol{\theta}_l^+ - \boldsymbol{\theta}_l^-)$ reduced by a factor of $\theta_l^\pm \sim 2^l b\tau$ (deduced by induction from $\theta_1^\pm \sim 2b\tau$). The decoherence is reduced by an order of $b^2 \tau_l^2$ at τ_l for each additional level of concatenation till saturation at the level $l_0 \approx -\log_2(b\tau)$. Hence, the coherence echo magnitude scales with the echo delay time according to $\exp(-(\tau_l/T_l)^{2l+2})$ as shown in Fig. 2(e). Our result shows the protection of electron spin coherence by pulse sequences with interpulse interval up to $\sim 10\mu s$

In conclusion, we note that our scheme of restoring the coherence depends on the pure decoherence being driven by the interaction in the spin bath and by the domination of the bath pair excitation in the slow bath dynamics. The pulse sequence design is borrowed from the dynamical decoupling schemes in NMR spectroscopies [10] and in quantum computation [4] but the disentanglement method aims directly at the bath dynamics. Our method seeks not to eliminate the object-bath interaction by dynamical averaging, but to disentangle

by controlling the quantum object to maneuver the bath evolution. Thus, elimination of coupling between the quantum object and the bath is not a necessary condition for their disentanglement, as illustrated by coherence recovery at $t = \sqrt{n(n+1)}\tau$ where effective object-bath interaction does not vanish even in the first order of hyperfine coupling \mathcal{A}/N . Direct observation of coherence echoes at such magic times is possible with the narrowing of inhomogeneous distribution by measurement projection [26]. The control of bath spins may well develop into a valuable addition to the collection of armaments of coherence preservation for quantum information processing.

We acknowledge support from NSF DMR-0403465, ARO/LPS, and DARPA/AFOSR.

-
- [1] W. H. Zurek, Rev. Mod. Phys. **75**, 715 (2003).
 - [2] E. Joos, H. D. Zeh, C. Kiefer, D. Giulini, J. Kupsch, and I.-O. Stamatescu, *Decoherence and the Appearance of a Classical World in Quantum Theory* (Springer, New York, 2003), 2nd ed.
 - [3] M. Schlosshauer, Rev. Mod. Phys. **76**, 1267 (2004).
 - [4] K. Khodjasteh and D. A. Lidar, Phys. Rev. Lett. **95**, 180501 (2005).
 - [5] L. Viola and S. Lloyd, Phys. Rev. A **58**, 2733 (1998).
 - [6] L. Viola and E. Knill, Phys. Rev. Lett. **94**, 60502 (2005).
 - [7] L. M. Duan and G. C. Guo, Phys. Rev. Lett. **79**, 1953 (1997); P. Zanardi and M. Rasetti, Phys. Rev. Lett. **79**, 3306 (1997); D. A. Lidar, I. L. Chuang, and K. B. Whaley, Phys. Rev. Lett. **81**, 2594 (1998).
 - [8] M. A. Nielsen and I. L. Chuang, *Quantum Computation and Quantum Information* (Cambridge University Press, Cambridge, 2000).
 - [9] F. Buscemi, G. Chiribella, and G. M. D'Ariano, Phys. Rev. Lett. **95**, 090501 (2005).
 - [10] C. P. Slichter, *Principles of Magnetic Resonance* (Springer-Verlag, New York, 1992), 3rd ed.
 - [11] N. V. Prokof'ev and P. C. E. Stamp, Rep. Prog. Phys. **63**, 669 (2000).
 - [12] D. Loss and D. P. DiVincenzo, Phys. Rev. A **57**, 120 (1998).
 - [13] A. Imamoglu, D. D. Awschalom, G. Burkard, D. P. DiVincenzo, D. Loss, M. Sherwin, and A. Small, Phys. Rev. Lett. **83**, 4204 (1999).
 - [14] W. A. Coish and D. Loss, Phys. Rev. B **70**, 195340 (2004).
 - [15] W. M. Witzel, R. de Sousa, and S. Das Sarma, Phys. Rev. B **72**, 161306(R) (2005).

- [3] W. Yao, R. B. Liu, and L. J. Sham, cond-mat/0508441 (2005).
- [17] T. Fujisawa, D. G. Austing, Y. Tokura, Y. Hirayama, and S. Tarucha, *Nature* **419**, 278 (2002).
- [18] J. M. Elzerman, R. Hanson, L. H. Willems van Beveren, B. Witkamp, L. M. K. Vandersypen, and L. P. Kouwenhoven, *Nature* **430**, 431 (2004).
- [19] M. Kroutvar, Y. Ducommun, D. Heiss, M. Bichler, D. Schuh, D. Abstreiter, and J. J. Finley, *Nature* **432**, 81 (2004).
- [20] The orbital wavefunction of the electron covers all N nuclei, so the contact hyperfine coupling with each nuclear spin is \mathcal{A}/N , inverse proportional to the bath size N .
- [21] A. M. Tyryshkin, S. A. Lyon, A. V. Astashkin, and A. M. Raitsimring, *Phys. Rev. B* **68**, 193207 (2003).
- [22] J. R. Petta, A. C. Johnson, J. M. Taylor, E. A. Laird, A. Yacoby, M. D. Lukin, C. M. Marcus, M. P. Hanson, and A. C. Gossard, *Science* **309**, 2180 (2005).
- [23] F. H. L. Koppens, C. Buizert, K. J. Tielrooij, I. T. Vink, K. C. Nowack, T. Meunier, L. P. Kouwenhoven, and L. M. K. Vandersypen, *Nature* **442**, 766 (2006).
- [24] A. S. Bracker, E. A. Stinaff, D. Gammon, M. E. Ware, J. G. Tischler, A. Shabaev, A. L. Efros, D. Park, D. Gershoni, V. L. Korenev, and I. A. Merkulov, *Phys. Rev. Lett.* **94**, 047402 (2005).
- [25] W. K. Rhim, A. Pines, and J. S. Waugh, *Phys. Rev. Lett.* **25**, 218 (1970).
- [26] G. Giedke, J. M. Taylor, D. D'Alessandro, M. D. Lukin, and A. Imamoglu, quant-ph/0508144 (2005); D. Klauser, W. A. Coish, and D. Loss, *Phys. Rev. B* **73**, 205302 (2006); D. Stepanenko, G. Burkard, G. Giedke, and A. Imamoglu, *Phys. Rev. Lett.* **96**, 136401 (2006).

Supplementary Information for “Restoring Coherence Lost to a Slow Interacting Mesoscopic Bath”

Pseudo-spin model

We give the salient points of the method of solving the electron nuclear spin dynamics in a GaAs quantum dot. The system consists of an electron with spin vector $\hat{\mathbf{S}}_e$ and N nuclear spins, $\hat{\mathbf{J}}_n$, with Zeeman energies Ω and ω_n under a magnetic field B_{ext} , respectively, where n denotes both positions and isotope types (^{75}As , ^{69}Ga and ^{71}Ga). The interaction can be separated as “diagonal” (or “longitudinal”) terms which involve only the spin vector components along the field (z) direction and “off-diagonal” (or “transverse”) terms which involve spin flips. Because Ω is much larger than ω_n and the strength of the direct nuclear-nuclear interactions (e.g., nuclear dipolar interaction), the off-diagonal part of the electron nuclear hyperfine interaction can be eliminated by a standard canonical transformation, with the second-order correction left as the hyperfine-mediated nuclear-nuclear interaction. For the same reason, the off-diagonal part of the nuclear-nuclear interaction includes only terms which conserve the Zeeman energies, thus excluding the hetero-nuclear terms. The total effective Hamiltonian can be written as $\hat{H} = \hat{H}_e + \hat{H}_N + \sum_{\pm} |\pm\rangle \hat{H}^{\pm} \langle \pm|$, with $\hat{H}_e = \Omega \hat{S}_e^z$, $\hat{H}_N = \omega_n \hat{J}_n^z$, $\hat{H}^{\pm} = \pm \hat{H}_A + \hat{H}_B + \hat{H}_D \pm \hat{H}_E$, and

$$\hat{H}_A = \sum'_{n \neq m} \frac{a_n a_m}{4\Omega} \hat{J}_n^+ \hat{J}_m^- \equiv \sum'_{n \neq m} A_{n,m} \hat{J}_n^+ \hat{J}_m^-, \quad (3a)$$

$$\hat{H}_B = \sum'_{n \neq m} B_{n,m} \hat{J}_n^+ \hat{J}_m^- \quad (3b)$$

$$\hat{H}_D = \sum_{n < m} D_{n,m} \hat{J}_n^z \hat{J}_m^z \quad (3c)$$

$$\hat{H}_E = \sum_n (a_n/2) \hat{J}_n^z \equiv \sum_n E_n \hat{J}_n^z, \quad (3d)$$

where $|\pm\rangle$ are the eigenstates of \hat{S}_e^z , the summation with a prime runs over only the homo-nuclear pairs, the subscript A denotes the hyperfine mediated nuclear-nuclear interaction, B the off-diagonal part of the direct nuclear-nuclear interaction, D the diagonal part of the direct nuclear-nuclear interaction, and E the diagonal part of the contact electron-nuclear hyperfine interaction. The hyperfine energy, determined by the electron orbital

wavefunction, has a typical energy scale $E_n \sim a_n \sim \frac{\mathcal{A}}{N} \sim 10^6 \text{ s}^{-1}$ for a dot with about 10^6 nuclei [1], where \mathcal{A} is the hyperfine constant depending only on the element type. The direct nuclear-nuclear interaction, which is “short-ranged” (referred here as decaying no slower than dipolar), has the near-neighbor coupling $B_{n,m} \sim D_{n,m} \sim b \sim 10^2 \text{ s}^{-1}$. The hyperfine mediated interaction, which couples any two nuclear spins that are in contact with the electron and is associated with opposite signs for opposite electron spin states, has an energy scale dependent on the field strength, $A_{n,m} \sim \frac{A^2}{N^2 \Omega} 1\text{--}10 \text{ s}^{-1}$ for field $\sim 40\text{--}1 \text{ T}$. This hyperfine mediate interaction is differentiated from the “short-range” direct nuclear-nuclear interaction by the qualifier “infinite-range”. We work in the interaction picture defined by \hat{H}_e and \hat{H}_N in which the dynamics are determined by \hat{H}^\pm .

The basis set of the bath are eigenstates of \hat{H}_N : $\bigotimes_n |j_n\rangle$. In Eqn. (3), \hat{H}_D and \hat{H}_E are diagonal in this basis. The off-diagonal terms \hat{H}_A , \hat{H}_B are weak perturbations that will excite the bath initially on an arbitrary configuration $|\mathcal{J}\rangle \equiv |j_1\rangle \cdots |j_N\rangle$. The elementary excitations in the nuclear spin bath are pair-flip excitations created by operators $\hat{J}_m^+ \hat{J}_n^-$ in the reduced Hamiltonian. Starting from any initial nuclear configuration, the evolution of the nuclear spin states by these elementary excitations is of the hierarchy as shown in the left side of Fig. 3. We can regard the zeroth layer of this hierarchy, the initial state, as the ‘vacuum’ of the pair-flip excitations and layer n corresponds to n pair-flip excitations have been created. The state at time t is a linear superposition of all possibilities:

$$|\mathcal{J}(t)\rangle = C_{\mathcal{J}}(t)|\mathcal{J}\rangle + \sum_{m,n} C_{m,n}(t) \hat{J}_m^+ \hat{J}_n^- |\mathcal{J}\rangle + \sum_{l,p,m,n} C_{l,p,m,n}(t) \hat{J}_l^+ \hat{J}_p^- \hat{J}_m^+ \hat{J}_n^- |\mathcal{J}\rangle + \cdots \quad (4)$$

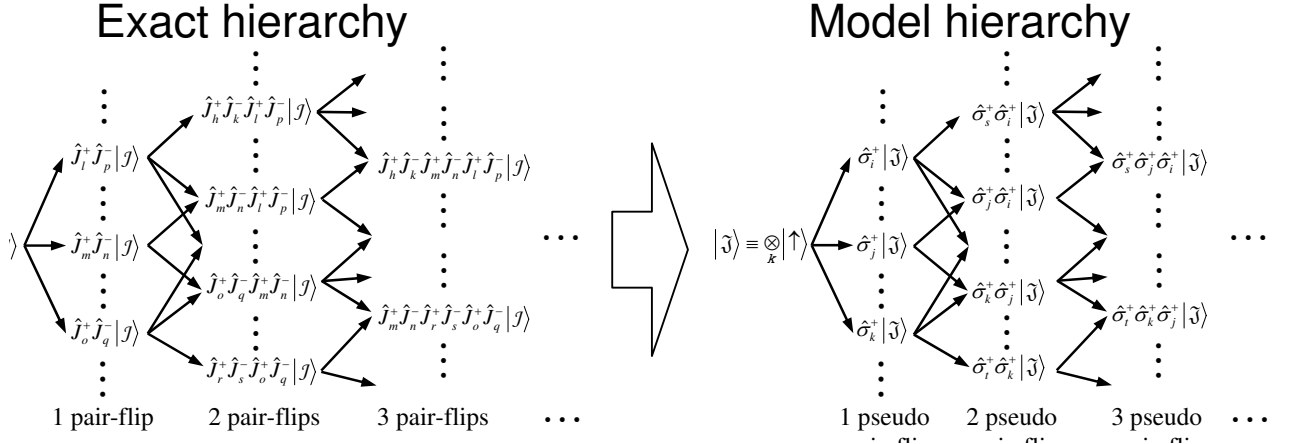


FIG. 3: Hierarchy of the nuclear spin dynamics.

where the summation over the indexes m, n, l, p, \dots are defined such that $|\mathcal{J}\rangle, \hat{J}_m^+ \hat{J}_n^- |\mathcal{J}\rangle, \hat{J}_l^+ \hat{J}_p^- \hat{J}_m^+ \hat{J}_n^- |\mathcal{J}\rangle, \dots$ denote different eigenstates of \hat{H}_N orthogonal to each other.

We solve this dynamics in the nuclear spin bath based on a pseudo-spin model as described below. We have, on sites labelled $n = 1, \dots, N$, the nuclear spin states $|j_n\rangle$ with $-j \leq j_n \leq j$ for nuclei of spin j . As the elementary excitations are pair dynamics driven by $\hat{J}_m^+ \hat{J}_n^-$, we first sort out the pair states $|j_n\rangle |j_m\rangle$. These pair states are divided into three categories:

1. *Down States*: A down state $|j_n\rangle |j_m\rangle$ has a partner $|j_n + 1\rangle |j_m - 1\rangle$ created by

$$\hat{J}_n^+ \hat{J}_m^- |j_n\rangle |j_m\rangle = \sqrt{(j + j_n + 1)(j - j_n)} \sqrt{(j - j_m + 1)(j + j_m)} |j_n + 1\rangle |j_m - 1\rangle$$

A down state must have $(j_n < j, j_m > -j)$. There are $(2j)^2$ down states for each bond.

2. *Up States*: An up state $|j_n\rangle |j_m\rangle$ has a partner $|j_n - 1\rangle |j_m + 1\rangle$ created by $\hat{J}_n^- \hat{J}_m^+ |j_n\rangle |j_m\rangle$. The up state must have $(j_n > -j, j_m < j)$. There are $(2j)^2$ up states for each bond.

3. *Bachelor States*: A single pair state has no partners connected by $\hat{J}_n^- \hat{J}_m^+ |j_n\rangle |j_m\rangle$ or its Hermitian conjugate, i.e., $j_n = j_m = j$ or $j_n = j_m = -j$.

The Bachelor states may be mapped to pseudo-spin 0 states. Since they are scalar states, their Hamiltonian terms will commute with every other operators, they can only contribute to the phase factor in the electron spin coherence through the Overhauser field, causing inhomogeneous broadening.

We shall find by an explicit construction that the up and down states can be paired to provide states of $(2j)^2$ two-level systems - the pseudo-spins. These states are divided into:

1. *Monogamy States*: Each state belongs to only one pseudo-spin although its partner may be a bigamist. These states are edge states in that at least one of the two spin quantum numbers (j_n or j_m) equal to $\pm j$ but they cannot both be equal to j or to $-j$. Half of them ($4j - 1$ states) are down states, $|j_n = -j\rangle |j_m > -j\rangle$ or $|j_n < j\rangle |j_m = j\rangle$, see Fig. 4(a). The other $4j - 1$ states, $|j_n > -j\rangle |j_m = -j\rangle$ or $|j_n = j\rangle |j_m < j\rangle$ are up states, see Fig. 4(c).

2. *Bigamy States*: Each belongs to two different pseudo-spins. They are interior states: $-j < j_n < j$ and $-j < j_m < j$. There are $(2j - 1)^2$ of them, see Fig. 4(b).

For a bond between two sites (n, m) , all possible pseudo-spins excitations are sort out

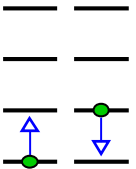
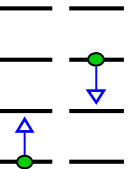
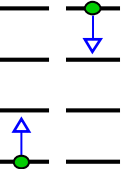
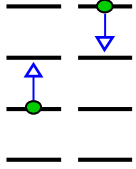
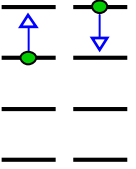
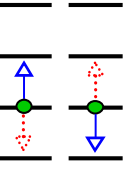
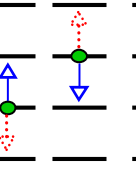
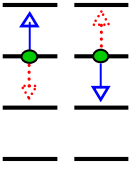
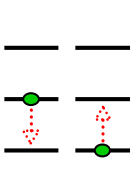
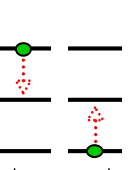
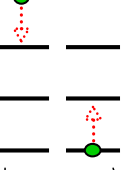
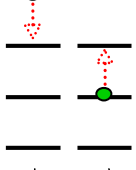
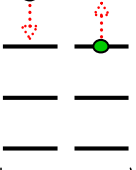
(a)	$j_n = -3/2$ $j_m = -1/2$ $u = -2$ $v = -1/2$  $ -2, -1/2, \downarrow\rangle$	$j_n = -3/2$ $j_m = 1/2$ $u = -1$ $v = -1$  $ -1, -1, \downarrow\rangle$	$j_n = -3/2$ $j_m = 3/2$ $u = 0$ $v = -3/2$  $ 0, -3/2, \downarrow\rangle$	$j_n = -1/2$ $j_m = 3/2$ $u = 1$ $v = -1$  $ 1, -1, \downarrow\rangle$	$j_n = 1/2$ $j_m = 3/2$ $u = 2$ $v = -1/2$  $ 2, -1/2, \downarrow\rangle$
(b)		$j_n = -1/2$ $j_m = -1/2$ $u = -1$ $v = 0$  $ -1, -1, \uparrow\rangle \otimes -1, 0, \downarrow\rangle$	$j_n = -1/2$ $j_m = 1/2$ $u = 0$ $v = -1/2$  $ 0, -3/2, \uparrow\rangle \otimes 0, -1/2, \downarrow\rangle$	$j_n = 1/2$ $j_m = 1/2$ $u = 1$ $v = 0$  $ 1, -1, \uparrow\rangle \otimes 1, 0, \downarrow\rangle$	
(c)	$j_n = -1/2$ $j_m = -3/2$ $u = -2$ $v = 1/2$  $ -2, -1/2, \uparrow\rangle$	$j_n = 1/2$ $j_m = -3/2$ $u = -1$ $v = 1$  $ -1, 0, \uparrow\rangle$	$j_n = 3/2$ $j_m = -3/2$ $u = 0$ $v = 3/2$  $ 0, 1/2, \uparrow\rangle$	$j_n = 3/2$ $j_m = -1/2$ $u = 1$ $v = 1$  $ 1, 0, \uparrow\rangle$	$j_n = 3/2$ $j_m = 1/2$ $u = 2$ $v = 1/2$  $ 2, -1/2, \uparrow\rangle$

FIG. 4: Illustration of construction of pseudo-spin states from a pair of nuclei of spin $3/2$. The solid dots show state $|j_n\rangle|j_m\rangle$. The solid arrows between lines show to which state the operator $\hat{J}_n^+ \hat{J}_m^-$ would lead and the dotted arrows show to which state $\hat{J}_n^- \hat{J}_m^+$ would lead. (a) Monogamy states which are mapped to pseudo-spin down: $|u, v, \downarrow\rangle$. (b) Bigamy states which are mapped to two pseudo-spins with one up and one down respectively: $|u, v - 1, \uparrow\rangle \otimes |u, v, \downarrow\rangle$ (c) Monogamy states mapped to pseudo-spins up: $|u, v - 1, \uparrow\rangle$.

and labelled by using two numbers $u(j_n, j_m)$ and $v(j_n, j_m)$ for $-j \leq j_n, j_m \leq j$,

$$\begin{aligned} u &= j_m + j_n \\ v &= \frac{1}{2}(j_n - j_m) \end{aligned} \quad (5)$$

The construction follows from the angular momentum addition of the two sites and is illustrated for $j = 3/2$,

$$\begin{array}{cccccc} u = & -3 & -2 & -1 & 0 & 1 & 2 & 3 \\ & & & & \frac{3}{2} & & & \\ & & & 1 & & 1 & & \\ & & \frac{1}{2} & & \frac{1}{2} & & \frac{1}{2} & \\ v = & 0 & & 0 & & 0 & & 0 \\ & & -\frac{1}{2} & & -\frac{1}{2} & & -\frac{1}{2} & \\ & & & -1 & & -1 & & \\ & & & & -\frac{3}{2} & & & \end{array} \quad (6)$$

When $u = \pm 2j$, the two-spin states are

$$|j_n\rangle|j_m\rangle = |j\rangle|j\rangle \quad \text{or} \quad | -j\rangle| -j\rangle. \quad (7)$$

Both are Bachelor states. For a u value equal to or between $-2j + 1$ and $2j - 1$, the v state at the bottom of the ladder is chosen to be the spin down of the doublet and one rung above to be its partner. Thus, the bottoms of the ladders yield the down monogamy states and the top rungs the up monogamy states. In between, the states are the bigamy states.

For any initial configuration $|\mathcal{J}\rangle$, the relevant set of pseudo-spins $\mathcal{G}_{\mathcal{J}}$ is determined by examining every possible nuclear spin pair (m, n) . Each pair will contribute 0, 1 or 2 pseudo-spins if $|j_m\rangle|j_n\rangle$ is in the Bachelor state, Monogamy state or Bigamy state configuration respectively (see Fig. 4). The many nuclear spin initial state $|\mathcal{J}\rangle$ is then replaced by,

$$|\mathcal{J}\rangle \equiv |j_1\rangle \cdots |j_N\rangle \Rightarrow |\mathfrak{J}\rangle \equiv \bigotimes_{k \in \mathcal{G}_{\mathcal{J}}} |k\sigma\rangle \quad (8)$$

where k labels both the nuclear pair (m, n) and the pseudo-spin type (u, v) . $\sigma = \uparrow$ or \downarrow

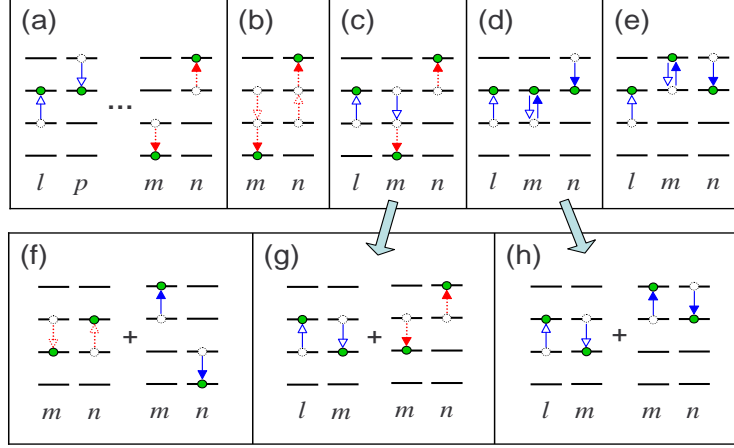


FIG. 5: Illustration of multi pair-flip excitations in the nuclear bath. We use hollow arrowheads to indicate the first pair-flip and solid arrowheads to indicate the second pair-flip. Dotted arrows denote the pseudo-spin flip from 'down' state to 'up' state and solid arrows for the inverse process (see text). (a) Independent pair flips; (b-e) Various situations of overlapping pair-flips; (f-h) Approximations in the independent pseudo-spin model.

depending on whether k is mapped from up or down Monogamy or Bigamy state. Different initial nuclear configurations will result in different sets of pseudo-spins. For a randomly chosen initial configuration $|\mathcal{J}\rangle$, the number of pseudo-spins is given by $M \sim (\frac{2j}{2j+1})^2 ZN$ where N is the total number of nuclear spins and Z the number of nuclei coupled to a particular nuclear spin by the nuclear-nuclear interaction. For short ranged direct interaction, $Z \sim O(10)$ and for the infinite-ranged hyperfine mediated interaction $Z = N$. The factor $(\frac{2j}{2j+1})^2$ arises as the single state, Monogamy state and Bigamy state are contributing 0, 1 and 2 pseudo-spins respectively. For convenience, when the set $\mathcal{G}_{\mathcal{J}}$ is determined from the $|\mathcal{J}\rangle$, we redefine the pseudo-spin up and down states, i.e. $|k, \sigma\rangle \rightarrow |k, -\sigma\rangle$, for those pseudo-spins in set $\mathcal{G}_{\mathcal{J}}$ so that the initial state $|\mathfrak{J}\rangle$ in this new definition corresponds to all pseudo-spins pointing 'up': $\bigotimes_k |\uparrow\rangle_k$. The redefinition is conditioned on the initial nuclear configuration $|\mathcal{J}\rangle$.

Conditioned on the electron state $|\pm\rangle$, the pseudo-spins are driven by the effective Hamiltonian of the form,

$$\hat{H}_{\text{sp}}^{\pm} = \sum_k \hat{\mathcal{H}}_k^{\pm} \equiv \sum_k \mathbf{h}_k^{\pm} \cdot \hat{\boldsymbol{\sigma}}_k / 2 \quad (9)$$

The effective magnetic field \mathbf{h}_k^{\pm} on the pseudo-spins, conditioned on the electron spin state, are to be determined by reproducing the matrix elements, $\langle \mathcal{J} | \hat{J}_m^+ \hat{J}_n^- \hat{H}^{\pm} \hat{J}_n^+ \hat{J}_m^- | \mathcal{J} \rangle - \langle \mathcal{J} | \hat{H}^{\pm} | \mathcal{J} \rangle$ and $\langle \mathcal{J} | \hat{H}^{\pm} \hat{J}_n^+ \hat{J}_m^- | \mathcal{J} \rangle$, namely the energy cost and transition matrix element for nuclear pair-

flips.

The pseudo-spin model for characterizing the nuclear spin bath dynamics is to approximate the exact evolution of Eqn. (4) by the independent evolution of all pseudo-spins in $\mathcal{G}_{\mathcal{J}}$,

$$|\mathfrak{J}(t)\rangle = \bigotimes_{k \in \mathcal{G}_{\mathcal{J}}} |\psi_k^{\pm}(t)\rangle = C_{\mathfrak{J}}(t)|\mathfrak{J}\rangle + \sum_{k_1} C_{k_1}(t)\hat{\sigma}_{k_1}^+|\mathfrak{J}\rangle + \sum_{k_1, k_2} C_{k_1, k_2}(t)\hat{\sigma}_{k_1}^+\hat{\sigma}_{k_2}^+|\mathfrak{J}\rangle + \dots \quad (10)$$

This pseudo-spin dynamics can be put into a similar hierarchy as shown in the right part of Fig. 3 which we will refer to as model hierarchy in contrast to the exact hierarchy.

With the mapping established for the state (Eqn. (8)) and the Hamiltonian (Eqn. (9)), the first two layers of the exact hierarchy will be reproduced exactly by the model hierarchy, i.e., there is a one to one correspondence between $\hat{J}_m^+\hat{J}_n^-|\mathcal{J}\rangle$ and $\hat{\sigma}_k^+|\mathfrak{J}\rangle$ with the energy and coupling to the initial state $|\mathcal{J}\rangle$ ($|\mathfrak{J}\rangle$) exactly reproduced.

Difference between the model and the exact hierarchies arises when more than one excitations have been created in the system. In Fig. 5, we illustrate with the case when two pair-flip excitations have been created. If the two pair-flips do not overlap as shown in Fig. 5(a), their dynamics are then independent of each other and well described by the pseudo-spin model. Fig.5(b-e) illustrate the various situations that the two pair-flips overlap, by sharing one or two nuclei. The flip-flop of the first nuclear pair (l, m) changes the spin configuration of both nuclear l and m and if a second flip-flop is to take place on pair (l, m) or (n, m) or (l, n) , it is no longer described by the dynamics of the original pseudo-spins assigned to it. Instead, in the model hierarchy by the independent pseudo-spin model, two successive flip-flops on pair (l, m) or two successive flip-flops on pair (l, m) and (m, n) respectively are shown in Fig.5(f-h). Fig. 5(g) can be considered as the approximate form of Fig. 5(c) and Fig. 5(h) as that of Fig. 5(d). The model hierarchy contains events like Fig. 5(f) which is absent in the exact hierarchy and events like Fig. 5(e) in the exact hierarchy is not contained in the model hierarchy. Therefore, on layer 2, the model hierarchy coincides with the exact hierarchy in events described by Fig. 5(a) and differ by replacing the events of Fig.5(b-e) with events of Fig.5(f-h). The difference in a general layer can be analyzed in the same way.

By the pseudo-spin model, we are using Eqn. (10) as the bath state at time t for calculating physical properties instead of Eqn. (4). The difference of the exact and model hierarchies is estimated below which serves as an upper bound for error estimation (notice that the

physical properties of interest are not necessarily changed by replacing events of Fig.5(b-e) with events of Fig.5(f-h), therefore, this error-estimation is not necessarily a tight bound). If $n - 1$ pair-flip excitations have already been generated, to create the next excitation, we have M pseudo-spin to choose from and $\sim 2(n - 1)Z$ of them overlap with the previous excitations. Therefore, the probability of having a new excitation without overlapping with the previous excitations is given by: $\sim \frac{M - 2(n-1)Z}{M}$. By induction, the probability of creating n non-overlapping pair-flip excitations is then given by,

$$\begin{aligned} p(n) &\simeq 1 \times \frac{M - 2Z}{M} \cdots \times \frac{M - 2(n-1)Z}{M} \\ &\simeq \exp \left[-\frac{2Z}{M} - \cdots - \frac{2(n-1)Z}{M} \right] \\ &= \exp \left[-\frac{n(n-1)}{N} \left(\frac{2j+1}{2j} \right)^2 \right] \end{aligned} \quad (11)$$

The second \simeq holds if $2nZ \ll M$ which is always true in the timescale relevant in our study.

Comparing the model hierarchy and the exact hierarchy, we find from the above analysis that they differ in layer n with the relative amount of $1 - p(n)$.

Error estimation

We perform a self-consistent analysis on validity of the pseudo-spin model. Here the relevant timescale plays the crucial role in determine the validity of the model. If only the first n layers of the hierarchy (the exact one and the model one) are involved, the error in the calculated physical properties is bounded by $1 - p(n) \ll 1$ if $n^2 \ll N$. Therefore, in the very short time limit, only the first several layers of the hierarchy can be involved and the pseudo-spin model gives an almost exact account of the dynamics. To estimate error upper bound for the longer time limit, we will calculate the number of layers involved (denoted as n) based on the model hierarchy of the pseudo-spin model. If n^2/N obtained is small, we conclude that n also faithfully reflects the number of layers involved in the exact hierarchy. Therefore, the error estimation based on the pseudo-spin model is faithful and any physical properties calculated based on pseudo-spin model is also a good approximation since the difference from the exact dynamics is small. Otherwise, the approximation is not good. It is established below that the condition $n^2 \ll N$ is the origin of an upper bound and a lower

bound on the quantum dot size N for which our theory is able to deal with. The validity of the pair-correlation approach (pseudo-spin model) is indeed in the mesoscopic regime.

At any given time t , an average excitation number $N_{flip}(t)$ can be defined as follows based on the model hierarchy,

$$N_{flip}(t) = 1 \times \sum_{k_1} |C_{k_1}(t)|^2 + 2 \times \sum_{k_1, k_2} |C_{k_1, k_2}(t)|^2 + 3 \times \sum_{k_1, k_2, k_3} |C_{k_1, k_2, k_3}(t)|^2 + \dots \quad (12)$$

and our analysis [2] shows that the layer-distribution of population in the hierarchy is of a normal distribution centered at N_{flip} , i.e. the population is distributed in layers from layer $N_{flip} - \sqrt{N_{flip}}$ to $N_{flip} + \sqrt{N_{flip}}$. Therefore, the quantity for characterizing the error upper bound is of a very simple form: $P_{err}(t) \equiv 1 - \exp(-N_{flip}^2(t)/N)$.

In the pseudo-spin model, $N_{flip}(t)$ defined in Eqn. (12) has an equivalent expression which is more convenient for evaluation:

$$N_{flip}(t) = \sum_k |\langle \downarrow | U_k^\pm(t) | \uparrow \rangle|^2 \quad (13)$$

where $U_k^\pm(t) \equiv e^{-i\hat{\mathcal{H}}_k^\pm t}$ is the evolution operator for pseudo-spin k . The contribution can be divide into two parts: $N_{flip}(t) = N_{flip}^A(t) + N_{flip}^B(t)$. N_{flip}^A is the number of non-local pair-flip excitations and N_{flip}^B is the number of local pair-flip excitations that have been created. $N_{flip}^A(t)$ and $N_{flip}^B(t)$ have very different behavior and we analyze them separately.

In free-induction evolution, the number of non-local pair-flip excitations is given by,

$$N_{flip}^A(t) = \sum_k \left(\frac{2A_k}{h_k^A} \right)^2 \sin^2 \frac{h_k^A t}{2} \leq \sum_k A_k^2 t^2 \simeq M_A \frac{\mathcal{A}^4}{N^4 \Omega^2} t^2 \simeq \frac{\mathcal{A}^4}{N^2 \Omega^2} t^2$$

where $h_k^A \equiv \sqrt{E_k^2 + 4A_k^2}$ and $M_A \sim N^2$ is the number of non-local nuclear spin pairs. Since the evolution of the non-local pair-correlation is completely reversed by the π pulses, $N_{flip}^A(t)$ is also reversed and $N_{flip}^A = 0$ at each spin echo time. Therefore, $N_{flip}^A(t)$ does not accumulate in the pulse controlled dynamics and we just need to look at the maximum value of $N_{flip}^A(t)$ between echoes. For example, in the control with the equally spaced pulse sequence, in order to have the coherence well preserved or restored at spin echo time, the delay time between successive pulses is limited by $\tau \lesssim T_H$, where $T_H \simeq b^{-1/2} \mathcal{A}^{-1/2} N^{1/4}$ is the Hahn echo decay timescale and $\sim 10\mu s$ in GaAs [3]. Therefore, N_{flip}^A at any time is

bounded by $N_{flip}^A(\mathcal{O}(T_H))$ in this scenario. The estimate of the bound on N imposed by N_{flip}^A for the validity of our approach is therefore,

$$\left(\frac{\mathcal{A}^4}{N^2\Omega^2}T_H^2\right)^2 \frac{1}{N} \sim \frac{\mathcal{A}^6}{N^4\Omega^4b^2} \ll 1 \quad (14)$$

For GaAs fluctuation dot in a magnetic field of 10 Tesla, the above condition is well satisfied for $N \gtrsim 10^4$. Estimation for other controlling pulse sequences give a lower bound on N which is in the same order.

For the number of local pair-flip excitations, we have a similar expression in the free-induction evolution,

$$N_{flip}^B(t) = \sum_k \left(\frac{2B_k}{h_k^B}\right)^2 \sin^2 \frac{h_k^B t}{2} \leq \sum_k B_k^2 t^2 \simeq M_B b^2 t^2 \simeq \alpha N b^2 t^2$$

where $h_k^B \equiv \sqrt{E_k^2 + 4B_k^2}$ and $M_B \sim \alpha N$ is the number of local nuclear spin pairs. α (~ 10 in GaAs) is determined by number of local neighbors and the nuclear spin quantum number j . In contrast to the non-local pair dynamics, the local pair dynamics is *not* reversed under the influence of the electron spin flip and $N_{flip}^B(t)$ accumulates all through the time. Nonetheless, it turns out that $N_{flip}^B(t) \leq \sum_k B_k^2 t^2 \simeq \alpha N b^2 t^2$ holds for all scenarios of pulse controls being discussed. Therefore, the condition $(N_{flip}^B)^2/N \ll 1$ sets an upper bound on N : $N\alpha^2(bt)^4 \ll 1$, which depends on the time range t we wish to explore. Alternatively speaking, $(N_{flip}^B)^2/N \ll 1$ sets an upper bound on the time range t we can explore for some fixed N using the pseudo-spin model. We illustrate this bound using the following two examples.

1. If we wish to calculate the Hahn echo signal using the pseudo-spin model, we shall have $(\alpha N b^2 T_H^2)^2/N \ll 1$ where the Hahn echo decay time $T_H \approx b^{-1/2} \mathcal{A}^{-1/2} N^{1/4}$ [3]. Therefore, the upper bound on N is given by $N^2 \alpha^2 b^2 \mathcal{A}^{-2} \ll 1$. For GaAs quantum dot, this condition is well satisfied for $N \lesssim 10^8$.

2. For bath of an intermediate size in the allowed region of $\min[\sqrt{N}, N^4 b^2 \Omega^4 \mathcal{A}^{-6}] \gg 1 \gg \alpha^2 N^2 b^2 \mathcal{A}^{-2}$, e.g., a quantum dot of typical size $N \sim 10^5 - 10^6$ in our problem, $(\alpha N b^2 t^2)^2/N \ll 1$ is satisfied for a much longer time range $t \sim 10T_H \sim 100\mu s$.

In summary, for the pair-correlation approximation (or pseudo-spin model) to be valid, nuclear spin dynamics of local pair-flips imposes an upper bound on N while nuclear spin

dynamics of non-local pair-flips imposes a lower bound. Within this mesoscopic regime, the pair-correlation approximation is well justified. The error estimation is based on characterizing the difference in the Hilbert space structure of the exact dynamics and that of the pseudo-spin model and assuming this difference has a full influence on the electron spin coherence calculation. Therefore, the bound is not necessarily tight and it is possible that the pulse control methodology developed using the pseudo-spin model have actually a much larger validity regime. Investigation is underway.

-
- [1] D. Paget, G. Lampel, and B. Sapoval, Phys. Rev. B **15**, 5780 (1977).
 - [2] W. Yao, R. B. Liu, and L. J. Sham, unpublished data.
 - [3] W. Yao, R. B. Liu, and L. J. Sham, cond-mat/0508441 (2005).